Corrosion Inhibitor Release from Zn-Al-[PO_4^{3-}]-[CO_3^{2-}] Layered Double Hydroxide Nanoparticles

E. Alibakhshi[1,2], E. Ghasemi[3], M. Mahdavian*[1], B. Ramezanzadeh[1]

[1.] Department of Surface Coating and Corrosion, Institute for Color Science and Technology, P. O. Box: 16765-654, Tehran, Iran.

[2.] Department of Chemical Engineering, Payame Noor University, P.O. Box 19395-3697, Tehran, Iran.

[3.] Department of Inorganic Pigment and Glazes, Institute for Color Science and Technology, P. O. Box: 16765-654, Tehran, Iran.

ABSTRACT

Zn-Al layered double hydroxide (LDH) nanoparticles with carbonate as the charge balancing anion in the interlayer space were synthesized using co-precipitation method. Then, the carbonate base Zn-Al LDH nanoparticles were doped with phosphate ion via anion-exchange reaction to synthesize Zn-Al-[PO_4^{3-}]-[CO_3^{2-}]. The structure and composition were characterized by X-ray diffraction (XRD), Fourier transform infrared spectroscopy (FT-IR) and thermal gravimetric-differential thermal analysis (TG-DTA). Inductively coupled plasma-optical emission spectrometer (ICP-OES) was employed to measure the phosphate release ability of Zn-Al-[PO_4^{3-}]-[CO_3^{2-}] in the 3.5 wt% NaCl solution. Results showed that zinc cation can release along with phosphate anion during ion exchange process. Then, the corrosion inhibition of phosphate anion and zinc cation on mild steel specimens was assessed by electrochemical impedance spectroscopy (EIS) and polarization. Field emission-scanning electron microscopy (FE-SEM) was used to study the surface morphology of the mild steel specimens after exposure to the test solutions. The results indicated the significant impact of zinc and phosphorus concentration in test solution on the corrosion inhibition properties. Prog. Color Colorants Coat. 9 (2016), 233-248© Institute for Color Science and Technology.

1. Introduction

Application of organic coatings, anodic or cathodic protection, corrosion inhibitors and suitable design of structure are the common routes to protect metallic surfaces [1, 2]. Hexavalent chromates as potent inhibiting pigments are widely used to prevent corrosion for many years. However, the current regulation protruded by REACH (Registration, Evaluation, Authorization and Restriction of Chemicals) prohibits the use of hexavalent chromium in almost all sectors except the aerospace industry [3]. Feasible alternatives to chromates are zinc phosphate pigment and its

*Corresponding author: mahdavian-m@icrc.ac.ir

generations [4–6]. Inhibitive performance of these components is widely investigated in literature [7–11]. The investigations revealed that modified zinc phosphate could release stronger inhibitive species at higher concentration than zinc phosphate. In other words, it is repeatedly reported that modified zinc phosphate namely 2nd, 3rd and 4th generations can increase corrosion inhibitive performance of the coatings [5, 7]. However, introducing these components into the coating matrix could not provide efficient and long-term active corrosion inhibitive properties when the aggressive species penetrate to the metallic substrates.

Designing new materials with controlled and on demand release performance has been proposed to avoid chromates use in anticorrosive coatings and provide sufficient long term inhibitive performance [12–14]. According to the literature, one of the best suggested materials is layered double hydroxide (LDH) [15–17].

LDHs, which have hydrotalcite like structure, are known to have general formula $[M_{II_{(1-x)}} M_{III_x} (OH)_2]^{x+} (A^{n-})_{x/n} . m H_2 O$, where M^{n+} is metal cations (M^{2+}: Mg^{2+}, Zn^{2+}, Ni^{2+}, Co^{2+}, Ca^{2+}, Cu^{2+}; M^{3+}: Al^{3+}, Fe^{3+}, Ga^{3+}, Cr^{3+}) and A^{n-} interlayer anion is loaded in the hydrated interlayer galleries [18–21]. The isomorphic substitution of M^{2+} with M^{3+} in brucite-like layers ($M_{II}(OH)_2$) creates a positive layer charge, thus LDHs can accommodate charge-compensating anions in the interlayer region. LDHs have generated diverse scientific and technological fondness in many potential areas of applications such as catalysis, energy, environment and medicine. Owing to the unique host-guest structure, many of the inhibitors can be readily intercalated into the interlayer space of LDH via anion exchange and co-precipitation approaches [16, 22–24].

In the present work, we report the corrosion inhibitor release from Zn-Al-[PO_4^{3-}]-[CO_3^{2-}] LDH nanoparticles. For this purpose, co-precipitation method was selected for the synthesis of Zn-Al-carbonate LDH. Then, Zn-Al-phosphate LDH nanoparticles were prepared by ion-exchange method and characterized by XRD, FT-IR spectroscopy and TG-DTA. The inhibitor release ability of Zn-Al-phosphate LDH nanoparticles in the chloride-containing electrolyte was investigated by inductively coupled plasma-optical emission spectrometer (ICP-OES). The corrosion inhibition performance of the phosphate intercalated Zn-Al-LDH nanoparticles was studied based on the release ability of Zn and phosphate in solution by electrochemical impedance spectroscopy (EIS) and polarization tests in the 3.5wt% NaCl solution on the steel substrate.

2. Experimental
2.1.Materials
Zinc nitrate, aluminum nitrate, sodium carbonate, sodium phosphate tribasic dodecahydrate, zinc chloride and sodium hydroxide were obtained Commercially and all the materials were used as received without further purification.

2.2. Synthesis of Zn-Al LDHs
Zn-Al-CO_3^{2-} LDH nanoparticles were prepared using the co-precipitation route at room temperature (30 ±1°C) by drop wise addition of two solutions, one containing solutions of nitrate salts of Zn^{2+} and $Al^{3+}$and another containing Na_2CO_3 and NaOH. The Zn:Al ratio chosen for the synthesis was 2:1 to obtain stable layered compounds. In the first step, a 0.02 M Zn $(NO_3)_2.6H_2O$ and 0.01 M $Al(NO_3)_3.9H_2O$ solution (V=40 mL, pH=2.88) was slowly added to 0.02 M Na_2CO_3 (V=70 mL, pH=10.7) under vigorous stirring for 1.5 h. During this reaction, the pH was kept constant (9.8±0.3) by simultaneous addition of 0.2M NaOH. Afterward, the obtained slurry centrifuged and washed several times with boiled deionized water. The resultant slurry was finally dried at 70 °C in an oven.

Zn-Al-PO_4^{3-} LDH nanoparticles were prepared through anion-exchange method. Accordingly, carbonate anions intercalated in the synthesized LDHs nanoparticles (first step) were replaced by phosphate via an anion-exchange reaction (second step). The anion-exchange was carried out under nitrogen atmosphere and all the solutions were prepared using boiled deionized water in order to avoid contamination with carbonate anions.

For the anion-exchange reaction, a 0.4 M Na_3PO_4. $12H_2O$ aqueous solution (V=500 mL, pH=11) was prepared in which 0.5 g of Zn-Al-CO_3^{2-} LDHs was dispersed. The suspension was held at room temperature and constant stirring for 48 h. The pH values of phosphate containing solution measured using Metrohm 744 pH meter are reported in Table 1. As time passed, the pH of the solution was increased due to anion-exchange between carbonate and phosphate. Finally, the phosphate-intercalated LDHs powders were washed and centrifuged with boiled deionized water and then dried.

Table 1: The pH measurement results for the $Zn-Al-CO_3^{2-}$ in phosphate solution after 48h.

Time (h)	pH
0	11±0.01
2	11.1±0.05
4	11.5±0.01
6	11.6±0.01
8	11.7±0.06
24	11.8±0.02
48	11.8±0.02

2.3. Characterization

The powder X-ray diffraction (XRD) was performed using PW 1800 Philips X-ray spectrometer with Cu-Kα radiation (λ=1.54060 A) on the synthesized pigment over the 2θ range from 10-60° at the rate of 2.5°/min. FT-IR analysis was carried out on KBr disks in the region of 400–4000 cm^{-1} by Perkin Elmer-Spectrum One. The thermogravimetric-differential thermal analysis (TG-DTA) was performed on a Mettler Toledo TGA-851thermoanalyzer. The samples were examined under an air flow rate of 2.0×10^{-5} m^3/min at a scan rate of 10 °C/min.

2.4. The release ability of the ions

The release behavior of the phosphate ions loaded in the carbonate base Zn-Al LDHs nanoparticles was analyzed in 3.5% NaCl solution. Phosphate intercalated Zn-Al LDHs powder (50 mg) was dispersed in 3.5% NaCl solution (10 mL), and stirred in various time at a rate of 300 rpm. The amount of phosphate, zinc and aluminum ions released from the $Zn-Al-PO_4^{3-}$ LDHs nanoparticles was measured with ICP-OES. The analysis was carried out using the ICP-OES of Varian Company (Australia), model Vista-PRO. In addition, to determine the phosphate, zinc and aluminum content of $Zn-Al-PO_4^{3-}$ LDH, 50 mg the powder was dissolved in 10 mL of 1 M nitric acid, then the concentration of the elements was measured by ICP-OES.

2.5. Evaluation of the corrosion inhibitive properties

The corrosion inhibitive properties of the mild samples in 3.5% NaCl solution was investigated by means of EIS and polarization. $ZnCl_2$ and $Na_3PO_4.12H_2O$ were added to the test solutions in order to adjust the concentration of zinc cation and phosphate anion equal to that released from $Zn-Al-PO_4^{3-}$ LDHs. A blank solution of 3.5 wt% NaCl without pigment was also prepared to take into account as a reference solution. Then, the mild steel samples were immersed in the test solutions for 4 h at 25°C.

The EIS measurements were carried out employing Ivium Compactstat (Netherlands) in the three electrode cell containing Ag/AgCl (3M KCl), graphite and the mild steel (1 cm^2 area) as reference, counter and working electrodes, respectively. The EIS measurements were implemented at open circuit potential using 10 mV perturbation in a frequency range of 10 kHz-10 mHz after 1, 2, 3 and 4 h of immersion.

The polarization curves were obtained in a three electrode cell (like the one used in the EIS test) at sweep rate of 1 mV/s in the range of ±200 mV from open circuit potential (OCP). The measured spectra were analyzed using Iviumsoft software. The EIS and polarization measurements were carried out 3 times to ensure the repeatability of the measurements. The mild steel with the mass percent composition of C 0.19, Mn 1.39, S > 0.005, Si 0.42, Cu 0.04, Cr 0.03, Mo 0.02, Co 0.06 and Fe (balance) was used in this study.

2.6. Surface analysis of mild steel specimens after exposure to the test solutions

The mild steel panels with dimensions of 1 cm ×1 cm and thickness of 2 mm were immersed in 10 mL of test solutions for 4 h; afterwards, the samples were washed with distilled water and dried. The surface morphology and composition of specimens were evaluated using a field emission scanning electron microscopy coupled with energy dispersive x-ray spectroscopy (FE-SEM, EDS, Mira).

3. Results and discussions

3.1. Characterization

The structure of Zn-Al LDHs before and after anion exchange was characterized by XRD. The XRD patterns of $Zn\text{-}Al\text{-}CO_3^{2-}$ and $Zn\text{-}Al\text{-}PO_4^{3-}$ LDHs are shown in Figure 1.

Five diffraction peaks can be indexed as (003), (006), (012), (015) and (018) reflections of the Zn-Al LDH phase (JCPDS 00-048-1026) [25]. It can be seen that (003) and (006) diffraction peaks are very sharp, indicating a good LDH crystallization [26]. The intensity of all the peaks was decreased after phosphate exchange indicating a decrease in crystallinity upon intercalation of carbonate with phosphate. For $Zn\text{-}Al\text{-}CO_3^{2-}$, a peak was observed at 38°, which indicates the presence of carbonate in the interlayer [27]. Two diffraction peaks observed between 32° and 35° for $Zn\text{-}Al\text{-}PO_4^{3-}$ in Figure 1 can be related to the presence of ZnO as a minor phase compared to the reference pattern JCPDS 01-079-0206 [27, 28].

The basal spacing was estimated from the respective 003 reflection. The basal spacing values are 0.712 and 0.767 nm for $Zn\text{-}Al\text{-}CO_3^{2-}$ and $Zn\text{-}Al\text{-}PO_4^{3-}$ LDH, respectively. Taking into account that the thickness of LDH layer is 0.48 nm, the gallery height for phosphate doped Zn-Al-LDH was increased from 0.235 to 0.29 nm. It was confirmed that the phosphate anions were successfully loaded into the interlayer of LDH and exchanged with some carbonate anions. The obtained results for the LDHs are in agreement with those reported in the literature. The intercalation of phosphate into the LDH structure was analyzed by FT-IR spectroscopy. The FT-IR spectra of $Zn\text{-}Al\text{-}CO_3^{2-}$ and Zn-

$Al\text{-}PO_4^{3-}$ nanoparticles are shown in Figure 2.

As can be observed in the FT-IR spectra, a broad band at 3460 cm^{-1} could be attributed to OH stretching vibration due to the presence of a hydroxyl group in the LDH and/or a physically adsorbed water molecules The band at 1640 and 1500 cm^{-1} is due to H-O-H bending vibration of the interlayer water [29]. This is commonly observed in the LDHs nanoparticles.

For $Zn\text{-}Al\text{-}CO_3^{2-}$, the narrow absorption at 1370 cm^{-1} was due to the stretching mode of interlayer carbonate anions in a symmetric environment, and the band close to 860 cm^{-1} was resulted from the bending mode of the interlayer carbonate group [29].

The bands recorded at around 1035 cm^{-1} are due to the presence of phosphate in the LDH structure. In the case of $Zn\text{-}Al\text{-}PO_4^{3-}$, all the above mentioned characteristic bands can be seen for carbonate in depressed form. This may show that complete removal of carbonate from LDHs was not achieved during 48 h ion-exchange process. The appearance of vibrations related to carbonate anion may also be attributed to the CO_2 adsorption from the atmosphere during the filtration process and hence reconstitution of $Zn\text{-}Al\text{-}CO_3^{2-}$ LDH [30].

Other bands in the low wave numbers (450-800cm^{-1}) can be ascribed to the lattice vibration modes of O-M-O and M-O (M= Zn, Al) [31]. The FT-IR spectra support the presence of phosphate in the LDH structure, which is in good agreement with the XRD results. The thermal stability of the LDHs nanoparticles was evaluated by TG-DTA to characterize the phosphate and or carbonate in the LDH scaffold. Figure 3 depicts the TG-DTA results for $Zn\text{-}Al\text{-}CO_3^{2-}$ and $Zn\text{-}Al\text{-}PO_4^{3-}$ nanoparticles.
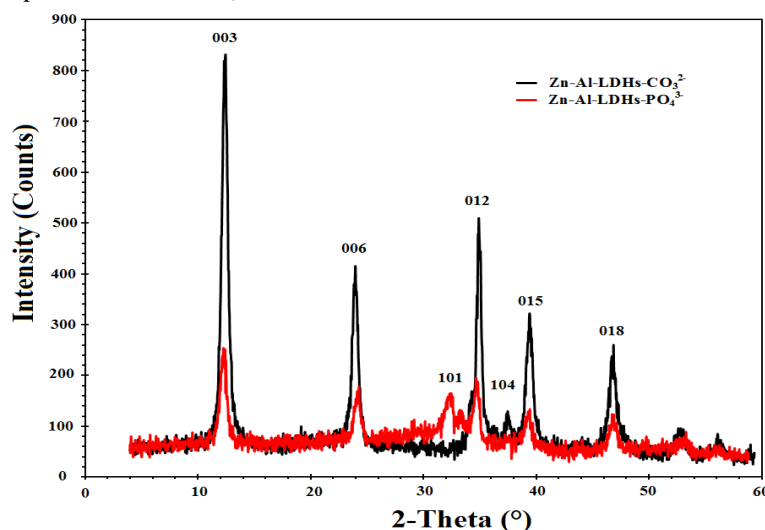
Figure 1: XRD patterns of $Zn\text{-}Al\text{-}CO_3^{2-}$ LDH and $Zn\text{-}Al\text{-}PO_4^{3-}$.
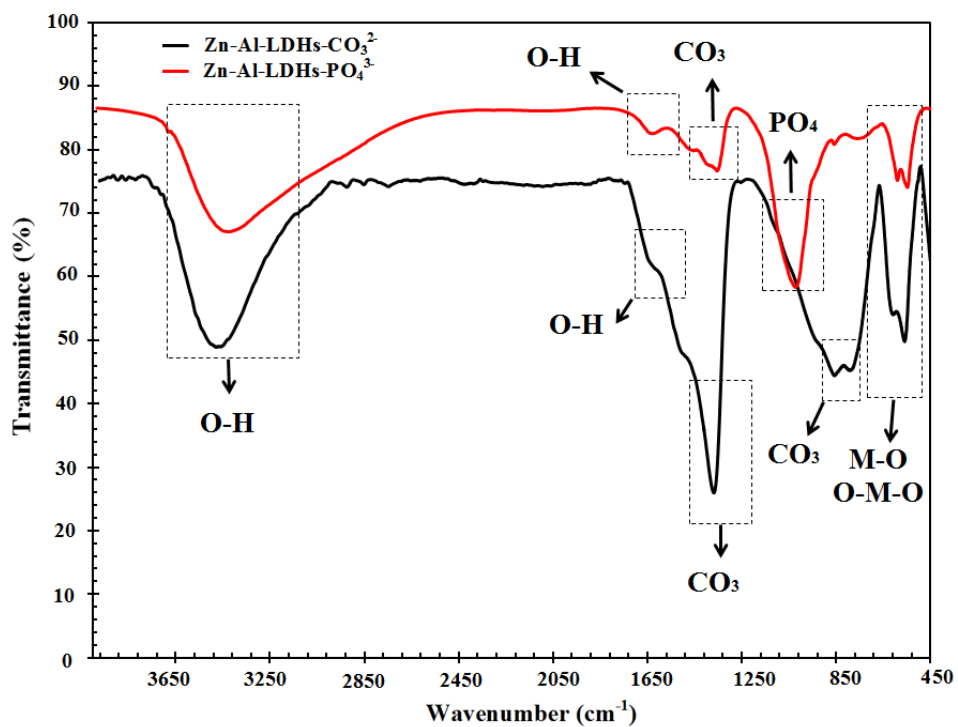
Figure 2: FT-IR spectra of the Zn-Al-CO$_3^{2-}$ LDH and Zn-Al-PO$_4^{3-}$.
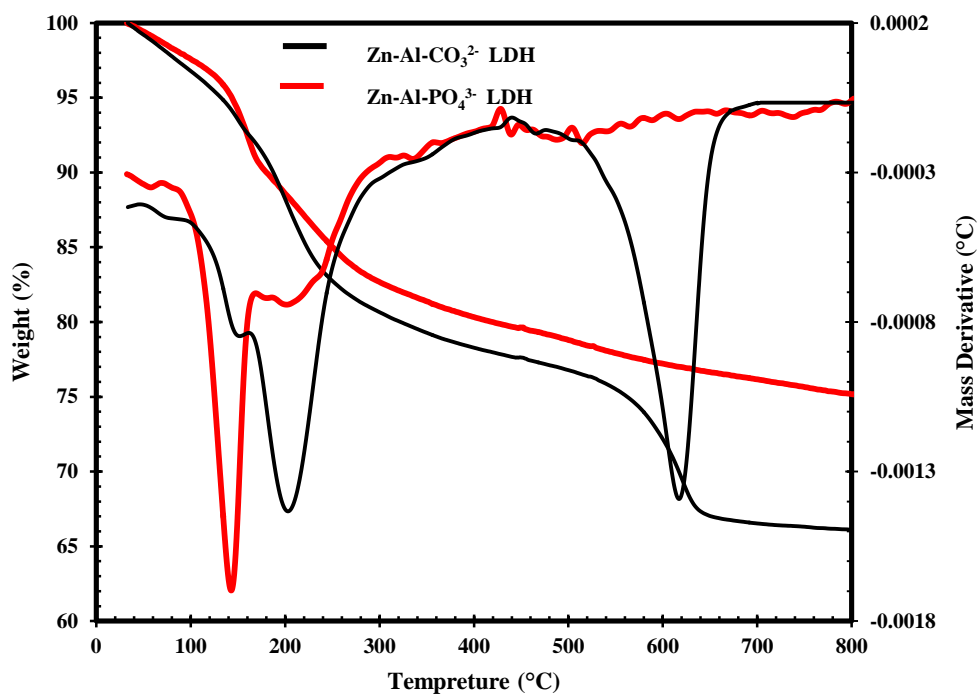

Figure 3: TG-DTA (b) curves of the Zn-Al-CO$_3^{2-}$ and Zn-Al-PO$_4^{3-}$ LDHs.

Three general steps of degradation can be observed for the Zn-Al-CO$_3$$^{2-}$ LDH. The first one (up to 160 °C) corresponds to the removal of physisorbed and interlayer water molecules. At higher temperatures, the major second stage (at around 200 °C) refers to the removal of water molecules by de-hydroxylation process. The last degradation stage (at around 620 °C) can be assigned to the decomposition of the carbonate ions in the interlayer.

The TG-DTA results for Zn-Al-PO$_4$$^{3-}$ showed three stages of weight loss. The weight losses were occurred at around 160, 220 and 250 °C corresponding to the removal of the interlayer water, de-hydroxylation and the phosphate anion polymerization, respectively. To better understand the possible polymerization of phosphate at 250 °C, the Zn-Al-PO$_4$$^{3-}$ was heated at 300°C for 20 min, and then the FT-IR spectroscopy was used to evaluate the change in the chemical structure. The FT-IR spectra are depicted in Figure 4.

Consistent with this idea, the FT-IR results exhibited a number of prominent sharp vibrational bands especially in the 850-1250 cm^{-1} in comparison with untreated sample. These bands include various P–O–P vibrations [32] with more intensity and sharpness, and clearly demonstrated the polymerization of phosphate groups in the LDH gallery. Interestingly, the peak around 620 °C in Zn-Al-CO$_3$$^{2-}$ is completely disappeared in Zn-Al-PO$_4$$^{3-}$ indicating complete

removal of carbonate anion during ion exchange reaction with phosphate anion. The thermogravimetric curves revealed complete decomposition of the carbonate at 650 °C. Considering the total weight loss at 650 °C, the Zn-Al-PO$_4$$^{3-}$ LDH shows around 10% lower degradation than Zn-Al-CO$_3$$^{2-}$ LDH which is attributed to the presence of phosphate anions.

3.2. The release behavior of the ions

Before discussing the release ability of phosphate in detail, let us recall that according to the pH of the solution, the possible predominant equilibrium for the phosphate ions is [33]:

$$H_3PO_4 \overset{(1)}{\Leftrightarrow} (H_2PO_4)^- + H^+ \overset{(2)}{\Leftrightarrow} (HPO_4)^{2-} + 2H^+ \overset{(3)}{\Leftrightarrow} (PO_4)^{3-} + 3H^+$$

The pH for the first step is between 2-3, for the second between 7-8 and for the third 11-13. Due to the pH used (11-11.82) in our synthesis, only the PO$_4$$^{3-}$ anions would be expected to be found in the Zn-Al LDHs layers [33].
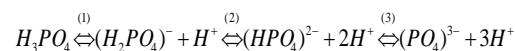
The phosphate, zinc and aluminum content of the Zn-Al-PO$_4$$^{3-}$ LDH, determined by ICP-OES, were 1.5, 1995 and 345 mg/L, respectively. The release behavior of the phosphate ions intercalated in the Zn-Al LDH nanoparticles was examined by monitoring the concentration of phosphate released in 3.5% NaCl solution using ICP-OES as a function of time (see Table 2).


Figure 4: FT-IR spectra of Zn-Al-PO$_4$$^{3-}$ without heat treatment and after heat treatment at 300 °C for 20 min.
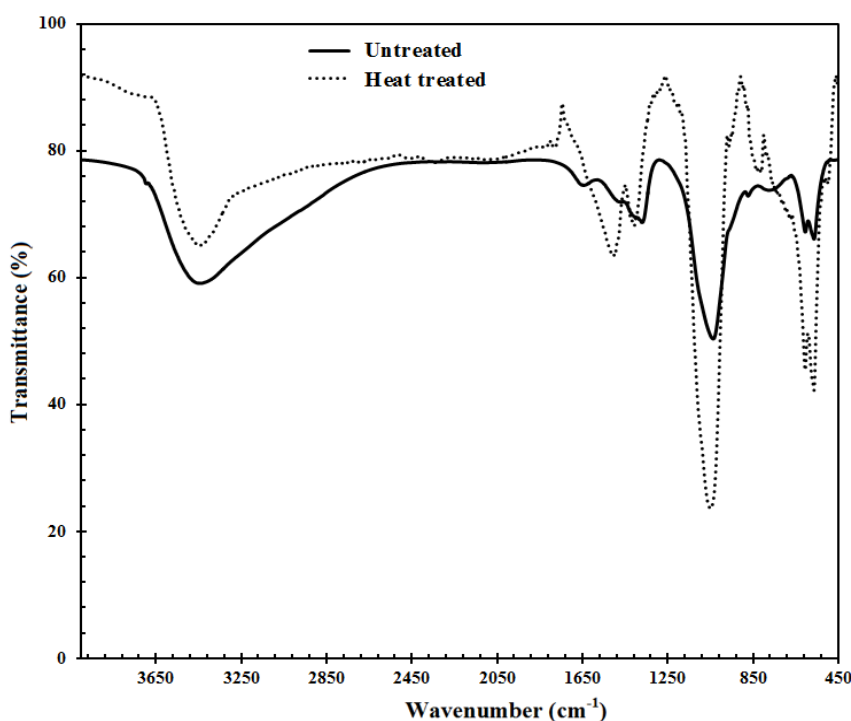
Table 2: Zinc, aluminum and phosphate release behavior for the phosphate intercalated Zn-Al LDHs.

Time (h)	Zn (mg/L)	Al (mg/L)	P (mg/L)
1	4.1	0.07	0.35
2	5.67	0.01	0.37
4	6.5	0.01	0.38
8	10.1	0.01	0.4
24	1.05	0.01	0.45
48	1.3	0.01	0.47

It was clear that release profile was a diffusion-controlled release process [34, 35]. As time passed, the phosphate release from the phosphate doped Zn-Al LDH nanoparticles was increased reaching to a constant concentration after 48 h. However, the concentration of zinc and aluminum released in the solution after 48 h was 1.3 and 0.01 mg/L, respectively. Comparison of the concentration of released zinc and aluminum with that of phosphate after 48 h which was about 0.47 mg/L reveals that the phosphate release in solution is governed by both ion-exchange and solubility equilibriums [36]. Zinc and aluminum release behavior for the phosphate intercalated Zn-Al LDHs are also listed in Table 2.

It was previously reported that the Zn-Al-LDHs containing polyoxometalate anions revealed Zn^{2+} ions loss during the ion exchange without destruction of the layered structure of the hydrotalcite [34]. Some aluminum ions are also released into solution, but the released percent of Al^{3+} was essentially less in comparison with phosphate and zinc. The corrosion inhibitive properties of phosphate and zinc in solution are explained in the next section.

3.3. Evaluation of the corrosion inhibitive properties

The corrosion inhibition properties of the mild steel samples in 3.5 wt% NaCl solution were conducted based on the release ability of Zn and phosphate in solution by EIS and polarization. The prepared samples with and without the addition of $ZnCl_2$ and $Na_3PO_4.12H_2O$ in 3.5 wt% NaCl solution are coded and displayed in Table 3. Figure 5 presents the typical Bode (a) and Nyquist (b) diagrams of the samples after 4 h of immersion in the test solutions.

The radius of semicircles in Nyquist plot is the largest for the samples immersed in the solutions labeled #3 and #4. Concurrently, the values of phase angle at high frequencies, which indicate the resistive-capacitive behavior of electrode-electrolyte system, are the most negative; and the values of the impedance magnitude at low frequencies, which approximate resistance at near DC current, are the highest for the samples immersed in the mentioned solutions. It is clear from Figure 5 that plots of the samples dipped in the solutions 1, 2, 5 and 6 include one relaxation time after 4 h immersion. However, second relaxation time was observed for the solution containing 3 and 4 after 4 h immersion. This can be attributed to the film growth on the surface of the steel specimen immersed in the solution labeled #3 and #4 [7].

Electrochemical equivalent circuits with one and two relaxation times were utilized in order to model the corrosion process. The typical fitting process is shown in Figure 6. In Figure 6, R_s, R_{ct}, R_f, CPE_{dl} and CPE_f are the solution resistance, the charge transfer resistance, the inhibitive film resistance, the constant phase element of the double layer and the constant phase element of the inhibitive film, respectively. The effective double layer (C_{dl}) and inhibitive film (Cf) capacitances were calculated according to Equation 1 [9, 37].

$$C = (Y_0 . R^{1-n})^{1/n} \qquad (1)$$

where C, Y, R and n represent capacitance of double layer or film, admittance of CPE elements of double layer or film, charge transfer resistance or film resistance and the empirical exponent of CPE elements of double layer or film, respectively. The electrochemical parameters extracted from impedance data are presented in Table 4.

Concerning the fitting results, the values of charge transfer resistance of the samples including zinc and phosphorus was considerably higher than the blank

solution. The highest charge transfer resistance was associated with the samples exposed to the test solution #4. In the case of charge transfer resistance, a trend correlation could be observed between the solution 4 and other extracts and blank solution. As time flied, the charge transfer resistance of the samples in solution #4 was incremented whereas a reverse trend was detected for other solutions. The upward trend is a reflection of the fact that corrosion inhibition was improved as time passed.

Table 3: The prepared samples with and without the addition of ZnCl$_2$ and Na$_3$PO$_4$.12H$_2$O in 3.5% wt. NaCl solution.

| Samples based on release ability	Coding	Na$_3$PO$_4$.12H$_2$O, 100 ppm (cc)	ZnCl$_2$, 100 ppm (cc)	NaCl (cc)
1 h	1	10.74	21.35	217.91
2 h	2	11.05	27.62	211.33
4 h	3	11.66	33.88	204.46
8 h	4	12.27	52.64	185.09
24 h	5	13.8	5.47	230.73
48 h	6	15.34	10.94	223.72
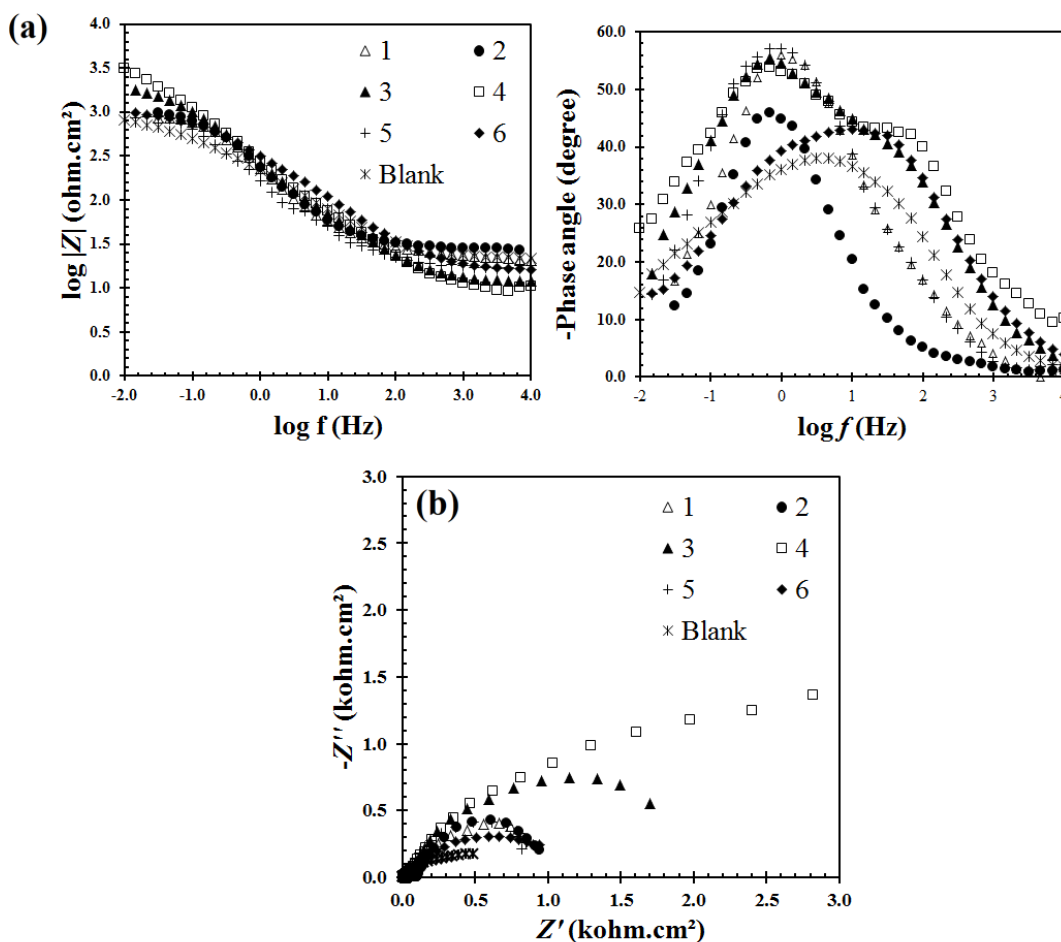
Figure 5: Typical Bode (a) and Nyquist (b) plots of the mild steel samples dipped in different test solutions (samples are defined in Table 3) for 4 h.

Table 4: The results obtained from fitting of EIS results (Figure 5) with the equivalent circuits shown in Figure 6.

| Solution	Time (h)	R_{ct} ($\Omega.cm^2$)	$Y_{0,dl}$ ($\mu s^n.\Omega^{-1}.cm^{-2}$)	n_{dl}	C_{dl} ($\mu F/cm^2$)	R_f ($\Omega.cm^2$)	$Y_{0,f}$ ($\mu s^n.\Omega^{-1}.cm^{-2}$)	n_f	C_f ($\mu F/cm^2$)	$\log |Z|$
Blank	1	1127.3	558.1	0.71	461.8	-	-	-	-	2.9
	2	910	493.4	0.69	344.3	-	-	-	-	2.87
	3	753.8	141.1	0.65	42.2	-	-	-	-	2.79
	4	681.4	92.1	0.64	19.4	-	-	-	-	2..7
1	1	1981	43.2	0.7	15.1	-	-	-	-	3.24
	2	1795	124.4	0.77	79.5	-	-	-	-	3.24
	3	1186	125.1	0.78	73	-	-	-	-	3.1
	4	896.4	259.4	0.84	196.5	-	-	-	-	2.9
2	1	2090	244	0.88	222.6	-	-	-	-	3.28
	2	1890	117.9	0.78	77.2	-	-	-	-	3.25
	3	1196	216.6	0.82	161	-	-	-	-	3.01
	4	920.4	218	0.84	160.5	-	-	-	-	2.96
3	1	2350	158.9	0.82	108.3	-	-	-	-	3.3
	2	2012	115.5	0.79	78.4	-	-	-	-	3.26
	3	1993	93	0.75	53	428.6	181.1	0.95	137.7	3.22
	4	1401	93.17	0.65	31.1	260.3	234.8	0.91	178.1	3.14
4	1	2465	216.6	0.82	188.72	-	-	-	-	3.49
	2	3814	179.5	0.62	142.3	222.5	158.6	0.96	138	3.5
	3	3920	94.3	0.63	52.6	504.6	124.5	0.95	107.6	3.5
	4	4371	47.4	0.64	19.5	75.5	96.1	0.84	37.6	3.55
5	1	1955	795.4	0.73	936.5	-	-	-	-	3.16
	2	1430	375.5	0.81	324.5	-	-	-	-	3.1
	3	1271	307.7	0.83	253.9	-	-	-	-	3
	4	1156	283.6	0.85	232.9	-	-	-	-	2.93
6	1	1758	264	0.83	225.6	-	-	-	-	3.2
	2	1744	269	0.84	232.9	-	-	-	-	3.19
	3	1435	80.37	0.73	36.1	-	-	-	-	3.08
	4	1245	3.49	0.55	0.04	-	-	-	-	2.99
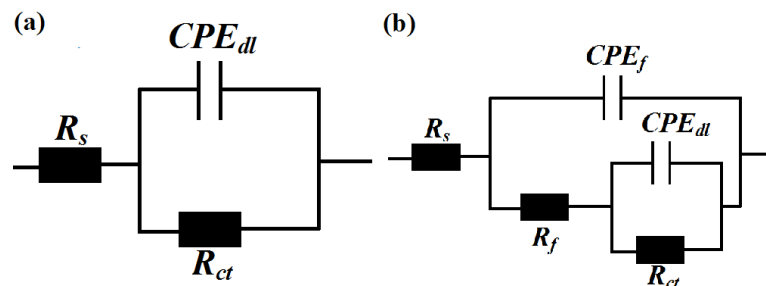
Figure 6: Equivalent circuits used to model experimental impedance data; (a) one-time constant equivalent circuits and (b) two-times constant.

Furthermore, comparison of the double layer capacitance of samples indicates that in the presence of zinc and phosphorus a considerable decrease could be observed, which is more pronounced for the samples immersed in the solutions #3, 4 and 6. These evolutions characterize the blocking increase in the extent of charge transfer at the steel surface and the decrease in the area of the contact surface related to passive film formation [38]. From Table 4, film resistance only appeared for the samples dipped in the solutions #3 and 4. This could be related to the development of a precipitated layer onto the surface.

Studying the impedance magnitude at low frequencies can present the general inhibitive properties, which can be directly read from the Bode diagrams without need for fitting and consequently without including the errors resulted from the fitting process [2, 39]. The impedance magnitude values at 100 mHz were obtained from the Bode plots and the results are given in Table 4. Values of the impedance magnitude at low frequencies show the same trend as that observed in values of charge transfer resistance. The trend of the impedance magnitude at low frequencies was ascending for the solution #4, while it was descending for other solutions. The solution #4 exhibits the highest impedance module at low frequency at all immersion times indicating that this sample provides better inhibition properties than other samples. The solution #3 takes second rank of

impedance module at low frequency.

It could be concluded that the addition of zinc and phosphorus to the solution led to a higher inhibition performance than blank solution. Further, the enhancement of the inhibition properties of solution #4 as compared to that of other solutions could be related to its higher zinc ion content, which led to a higher possibility of the formation of a protective layer on the mild steel surface.

Polarization test was done in order to further investigate the inhibition mechanism of the steel panels dipped in the solutions without and with addition of zinc and phosphate. Figure 7 compares the polarization test results for the samples immersed in different test solutions for 4 h. Polarization curves demonstrate the effect of zinc and phosphate on cathodic and particularly anodic current densities. As can be seen from the figure, introduction of zinc and phosphate resulted in corrosion potential shift to more positive values which could be related to anodic inhibition mechanism. From Figure 7, the corrosion potential shift is the more positive for the samples immersed in the solutions labeled #3 and 4.

The electrochemical parameters including corrosion potential (E_{corr}), corrosion current density (i_{corr}), anodic Tafel slope (b_a), cathodic Tafel slope (b_c) and polarization resistance (R_P) which were derived from the polarization curves by Tafel region extrapolation are listed in Table 5.

Table 5: Electrochemical parameters derived from polarization curves of the samples immersed in the test solutions after 4 h.

Solution	E_{corr} versus Ag/AgCl (mV)	i_{corr} (μA/cm^2)	b_a (V/dec)	b_c (V/dec)	R_P (Ω.cm^2)
Blank	-680	11.2	0.11	0.41	3102
1	-660	9.85	0.084	0.757	3334
2	-650	10.8	0.087	0.516	3410
3	-627.2	6.25	0.087	0.335	4883
4	-637.3	5.93	0.086	0.38	5061
5	-645.6	8.2	0.092	0.343	3881
6	-644	8.7	0.084	0.57	3570
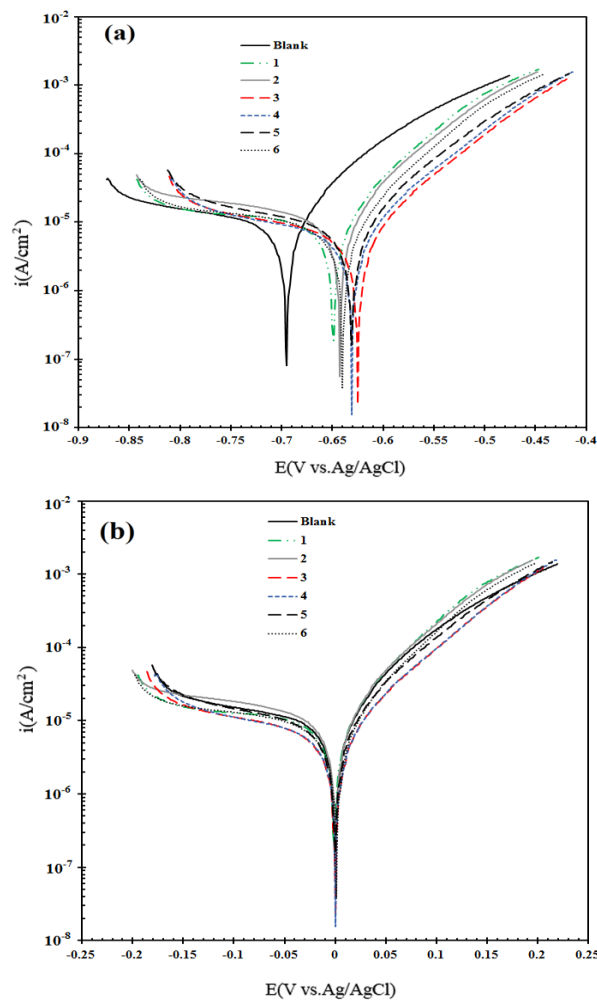
Figure 7: Polarization curves of mild steel samples after 4 h immersion in test solutions (samples are defined in Table 3): (a) as measured (b) shifted E_{corr} to zero potential to compare the anodic and cathodic branches at the same overpotential.

According to the results listed in Table 5, introducing zinc and phosphate into 3.5 wt% NaCl solutions caused decrease of the corrosion current density and increase of the corrosion potential and polarization resistance compared to the blank sample. This indicates that the extracts include zinc and phosphate prevented the steel against corrosion through formation of protective film on the active sites of the steel. The corrosion potential value of samples immersed in solution #3 after 4 h was higher than those immersed in other solutions. The solution #4 takes second rank of the corrosion potential value.

The lower current density and the higher polarization resistance were obtained in the solution # 4 compared to other solutions. These observations are completely in agreement with the results of EIS measurements. It was evident that the results of polarization tests were consistent with those of impedance measurements in which solution labelled #4 showed better performance in comparison with other solutions. It seems that the better inhibition performance of solution #4 in comparison with other solutions is related to the existence of higher amount of zinc and the presence of a high amount of phosphate in the solution.

3.4. Surface analysis of mild steel samples after exposure to test solutions

The morphology and composition of the films precipitated on the steel surface exposed to the solutions without and with zinc and phosphate were studied by FE-SEM. The SEM micrographs of different samples are shown in Figure 8.

As can be seen from the Figure 8, corrosion products are formed on the surface of the steel sample immersed in the blank solution. It can be also seen that lower corrosion products formed on the surface of the steel sample immersed in the solution containing zinc and phosphate compared to the one exposed in the blank solution. This observation emphasizes that the addition of zinc and phosphorus to solution protected the steel surface from corrosion.

SEM micrographs clearly illustrated a compact deposited on the samples #3 and 4. It is reasonable to assume that the presence of this deposited layer could be accounted for the better corrosion inhibition observed for the samples #3 and 4. Regarding to the EIS results there is definitely a protective film on the surface for these samples.

The chemical composition of the surface detected by FE-SEM is listed in Table 6. Considering the precision of the FE-SEM analysis, the layer formed on the steel surface was composed of Fe, Na, Cl, Zn and P elements. The presence of Na^+ at higher concentrations than Cl^- could be related to formation of anionic complexes on the surface, which is neutralized by Na^+ [40]. According to the high percentage of Na on the mild steel samples immersed in solutions #1, 3 and 5 (Table 6), it seems that formation of such complex is possible. However, for the samples exposed to solutions #2 and 6, the atomic percentage of Na is zero.

Table 6: The results of Fe-SEM analysis of the precipitated layers on the surface of steel samples after 4 h of immersion in 3.5% wt. NaCl solution including zinc and phosphor.

| Sample	Fe	Na	Cl	Zn	P
1	Balance	1.41	0.21	0.25	0.12
2	Balance	0	0.29	0.46	0.14
3	Balance	3.3	0.38	0.85	0.19
4	Balance	0.77	0.48	0.57	0.55
5	Balance	9.5	1.07	0.34	0.29
6	Balance	0	0.22	0.23	0.24
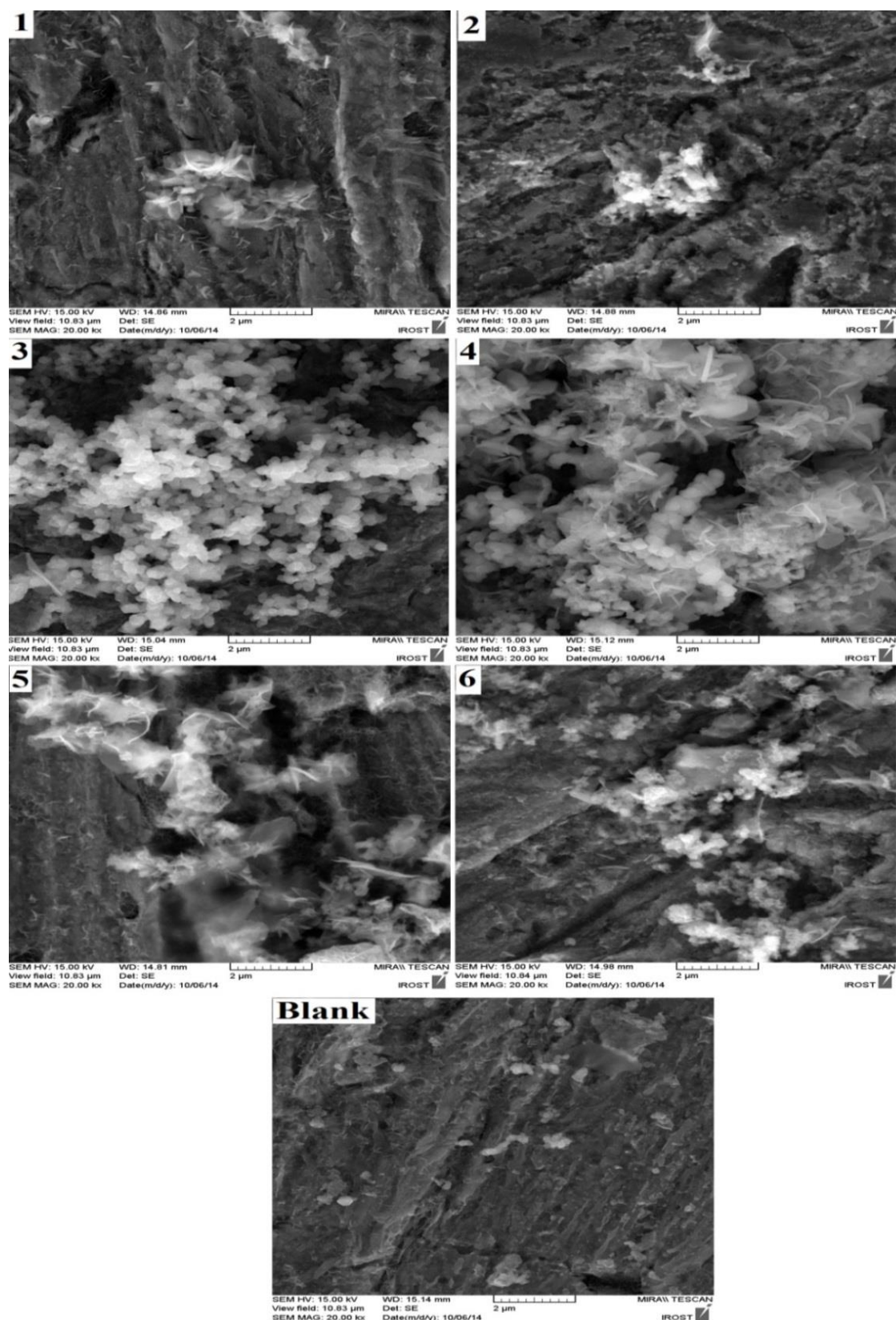
Figure 8: The FE-SEM micrographs of the mild steel surface after 4 h exposure to blank solution blank and prepared test solutions (samples are defined in Table 3).

It can be seen that more P component was detected on the surface of the steel sample immersed in the solution # 4 than the sample immersed in the other solution. This sample had the second rank of the Zn content on the surface. The higher concentration of P detected on the steel surface is a possible reason for the better inhibitive effect (section 3.3) of sample # 4 in comparison with other samples.

4. Conclusion

This work was devoted to study the corrosion inhibitive properties of carbonate base Zn-Al layered double hydroxides nanoparticles doped with phosphate ion. The results could be summarized as follow:

- XRD analysis exhibited an increase of gallery height which confirms the intercalation of phosphate anions into the interlayer of LDH and exchange with some carbonate anions.
- The intercalation between the phosphate and the positive charge of the LDH nanoparticles interlayers was also supported using FT-IR spectroscopy.
- ICP measurements depicted the increase of phosphorus content in NaCl solution as time elapsed.
- The EIS and polarization data indicated the significant impact of zinc and phosphorus content on the inhibition behavior of the solution.
- The elemental composition obtained from the FE-SEM revealed that the phosphate concentration in the surface film played a major rule in corrosion inhibition performance.
- As shown by electrochemical measurements and surface analysis, the solution #4 could offer better corrosion inhibition to the mild steel in 3.5 wt% NaCl solution.

Acknowledgements

5. References

1. E. Alibakhshi, E. Ghasemi, M. Mahdavian, A comparison study on corrosion behavior of zinc phosphate and potassium zinc phosphate anticorrosive pigments, *J. Prog. Color Colorants Coat.*, 5 (2012), 91–99.

2. E. Alibakhshi, E. Ghasemi, M. Mahdavian, Optimization of potassium zinc phosphate anticorrosion pigment by Taguchi experimental design, *Prog. Org. Coating.*, 76 (2013), 224–230.

3. M.F. Montemor, Functional and smart coatings for corrosion protection: A review of recent advances, *Surf. Coatings Technol.,* 258 (2014), 17–37.

4. A.C. Bastos, M.G. Ferreira, A.M. Simões, Corrosion inhibition by chromate and phosphate extracts for iron substrates studied by EIS and SVET, *Corros. Sci.*, 48 (2006) 1500–1512.

5. F. Askari, E. Ghasemi, B. Ramezanzadeh, M. Mahdavian, Synthesis and characterization of the fourth generation of zinc phosphate pigment in the presence of benzotriazole, *Dye. Pigment.,* 124 (2016), 18–26.

6. R. Naderi, M.M. Attar, The role of zinc aluminum phosphate anticorrosive pigment in Protective Performance and cathodic disbondment of epoxy coating, *Corros. Sci.*, 52 (2010), 1291–1296.

7. E. Alibakhshi, E. Ghasemi, M. Mahdavian, Sodium zinc phosphate as a corrosion inhibitive pigment, *Prog. Org. Coatings.*, 77 (2014), 1155–1162.

8. E. Alibakhshi, E. Ghasemi, M. Mahdavian, Evaluation of corrosion inhibition performance of synthesized potassium zinc phosphate pigments in two different conditions during immersion time, *J. Color Sci. Tech.,* 9 (2015), 113–123.

9. E. Alibakhshi, E. Ghasemi, M. Mahdavian, The influence of surface modification of lithium zinc phosphate pigment on corrosion inhibition of mild steel and adhesion strength of epoxy coating, *J. Sol-Gel Sci. Technol.*, 72 (2014), 359–368.

10. E. Alibakhshi, E. Ghasemi, M. Mahdavian, Corrosion inhibition by lithium zinc phosphate pigment, *Corros. Sci.*, 77 (2013), 222–229.

11. Y. Shao, C. Jia, G. Meng, T. Zhang, F. Wang, The role of a zinc phosphate pigment in the corrosion of scratched epoxy-coated steel, *Corros. Sci.*, 51 (2009), 371–379.

12. M.F. Montemor, D.V. Snihirova, M.G. Taryba, S.V. Lamaka, I.A. Kartsonakis, A.C. Balaskas, et al., Evaluation of self-healing ability in protective coatings modified with combinations of layered double hydroxides and cerium molibdate nanocontainers filled with corrosion inhibitors, *Electrochim. Acta.*, 60 (2012),

31–40.

13. A. Yabuki, K. Okumura, Self-healing coatings using superabsorbent polymers for corrosion inhibition in carbon steel, *Corros. Sci.*, 59 (2012), 258–262.

14. M. Serdechnova, S. Kallip, M.G.S. Ferreira, M.L. Zheludkevich, Active self-healing coating for galvanically coupled multi-material assemblies, *Electrochem. Commun.*, 41 (2014), 51–54.

15. E. Alibakhshi, E. Ghasemi, M. Mahdavian, B. Ramezanzadeh, Characterization of inhibitor release from hydrotalcite pigment, 6th Int. *Color Coat. Congr.*, (2015).

16. J. Tedim, S.K. Poznyak, A. Kuznetsova, D. Raps, T. Hack, M.L. Zheludkevich, et al., Enhancement of active corrosion protection via combination of inhibitor-loaded nanocontainers., ACS Appl. M*ater. Interfaces.*, 2 (2010), 1528–35.

17. M.L. Zheludkevich, J. Tedim, M.G.S. Ferreira, Smart coatings for active corrosion protection based on multi-functional micro and nanocontainers, *Electrochim. Acta.*, 82 (2012), 314–323.

18. J.-H. Syu, J.-Y. Uan, M.-C. Lin, Z.-Y. Lin, Optically transparent Li–Al–CO$_3$ layered double hydroxide thin films on an AZ31 Mg alloy formed by electrochemical deposition and their corrosion resistance in a dilute chloride environment, *Corros. Sci.*, 68 (2013), 238–248.

19. J. Tedim, A. Kuznetsova, A.N. Salak, F. Montemor, D. Snihirova, M. Pilz, et al., Zn–Al layered double hydroxides as chloride nanotraps in active protective coatings, *Corros. Sci.*, 55 (2012) 1–4.

20. T. Ishizaki, N. Kamiyama, K. Watanabe, A. Serizawa, Corrosion resistance of Mg(OH)2/Mg-Al layered double hydroxide composite film formed directly on combustion-resistant magnesium alloy AMCa602 by steam coating, *Corros. Sci.*, 92 (2015), 76–84.

21. J. Chen, Y. Song, D. Shan, E.-H. Han, Study of the corrosion mechanism of the in situ grown Mg–Al–CO3 hydrotalcite film on AZ31 alloy, *Corros. Sci.,* 65 (2012), 268–277.

22. S.K. Poznyak, J. Tedim, L.M. Rodrigues, A.N. Salak, M.L. Zheludkevich, L.F.P. Dick, et al., Novel inorganic host layered double hydroxides intercalated with guest organic inhibitors for anticorrosion applications., ACS *Appl. Mater. Interfaces.*, 1 (2009), 2353–62.

23. T.T.X. Hang, T.A. Truc, N.T. Duong, N. Pebre, M.G. Olivier, Layered double hydroxides as containers of inhibitors in organic coatings for corrosion protection of carbon steel, *Prog. Org. Coating.*, 74 (2012), 343–348.

24. V. Shkirskiy, P. Keil, H. Hintze-Bruening, F. Leroux, P. Vialat, G. Lefèvre, et al., Factors Affecting MoO$_4$$^{2-}$ Inhibitor Release from Zn$_2$Al Based Layered Double Hydroxide and Their Implication in Protecting Hot Dip Galvanized Steel by Means of Organic Coatings, ACS Appl. Mater. Interfaces. 7 (2015) 25180–25192.

25. E. Alibakhshi, E. Ghasemi, M. Mahdavian, B. Ramezanzadeh, S. Farashi, Fabrication and Characterization of PO$_4$$^{3-}$ Intercalated Zn-Al- Layered Double Hydroxide Nanocontainer, *J. Electrochem. Soc.,* 163 (2016), C495–C505.

26. J. Das, B.S. Patra, N. Baliarsingh, K.M. Parida, Adsorption of phosphate by layered double hydroxides in aqueous solutions, *Appl. Clay Sci.*, 32 (2006), 252–260.

27. M. Mamat, K. Halim, K. Bulat, M. Aidil, A. Abdullah, A. Rahman, Zinc aluminium carbonate layered double hydroxide: syntheses and characterization, *J. Ultra Chem.*, 7 (2011), 430–435.

28. R. Frost, A. Musumeci, T. Kloprogge, M. Adebajo, M. Wayde, Raman spectroscopy of hydrotalcites with phosphate in the interlayer implications for the removal of phosphate from water. Journal of Raman Spectroscopy., 37 (2006), 733–741.

29. J. Liu, J. Song, H. Xiao, L. Zhang, Y. Qin, D. Liu, et al., Synthesis and thermal properties of ZnAl layered double hydroxide by urea hydrolysis, *Powder Technol.*, 253 (2014), 41–45.

30. R. Anbarasan, W.D. Lee, S. Im, Adsorption and intercalation of anionic surfactants onto layered double hydroxides : XRD study, *Bull. Mater. Sci.*, 28 (2005), 145–149.

31. P. Ding, B. Qu, Synthesis and characterization of exfoliated polystyrene/ZnAl layered double hydroxide nanocomposite via emulsion polymerization., *J. Colloid Interface Sci.*, 291 (2005), 13–18.

32. M. Badreddine, A. Legrouri, A. Barroug, A. De Roy, J.P. Besse, Ion exchange of different phosphate ions into the zinc–aluminium–chloride layered double hydroxide, *Mater. Lett.*, 38 (1999), 391–395.

33. A. Legrouri, M. Badreddine, A. Barroug, A. Deroy, Besse, Influence of pH on the synthesis of the Zn – Al – nitrate layered double hydroxide and the exchange of nitrate by phosphate ions, *J. Mater. Sci. Lett.,* 8 (1999), 1077–1079.

34. S.P. V Mahajanam, R.G. Buchheit, Characterization of inhibitor release from Zn-Al- [V10 O28] 6– hydrotalcite pigments and corrosion protection from hydrotalcite pigmented epoxy coatings, *Corrosion.*, 64

(2008), 230–240.

35. M. a. Woo, T.W. Kim, M.J. Paek, H.W. Ha, J.H. Choy, S.J. Hwang, Phosphate-intercalated Ca–Fe-layered double hydroxides: Crystal structure, bonding character, and release kinetics of phosphate, *J. Solid State Chem.*, 184 (2011), 171–176.

36. M.L. Zheludkevich, S.K. Poznyak, L.M. Rodrigues, D. Raps, T. Hack, L.F. Dick, et al., Active protection coatings with layered double hydroxide nanocontainers of corrosion inhibitor, *Corros. Sci.,* 52 (2010), 602–611.

37. B. Hirschorn, M.E. Orazem, B. Tribollet, V. Vivier, I. Frateur, M. Musiani, Determination of effective capacitance and film thickness from constant-phase-element parameters, *Electrochim. Acta.*, 55 (2010), 6218–6227.

38. F. Simescu, H. Idrissi, Effect of zinc phosphate chemical conversion coating on corrosion behaviour of mild steel in alkaline medium: protection of rebars in reinforced concrete, *Sci. Technol. Adv. Mater.*, 9 (2008), 045009.

39. M. Zubielewicz, W. Gnot, Mechanisms of non-toxic anticorrosive pigments in organic waterborne coatings, *Prog. Org. Coatings*., 49 (2004), 358–371.

40. M. Mahdavian, R. Naderi, Corrosion inhibition of mild steel in sodium chloride solution by some zinc complexes, *Corros. Sci.*, 53 (2011), 1194–1200.